

**EVALUATION OF THE RF EMISSION AND EXPOSURE OF
HUMANS TO THE AT&T WIRELESS SERVICES FIXED
WIRELESS RU ANTENNA IN TERMS OF COMPLIANCE
WITH FCC GENERAL POPULATION RF EXPOSURE
STANDARDS**

January 12, 1999

A Report Prepared for Mr. Keith Peavler
Senior EMC Engineer
Strategic Technology Group
AT&T Wireless Services
Redmond, Washington 98073-9759

By

Arthur W. Guy, Ph.D.
Bioelectromagnetics Consulting
18122 60th PL NE
Kenmore, Washington 98028

TABLE OF CONTENTS

EXECUTIVE SUMMARY.....	1
1 INTRODUCTION.....	4
2 COMPUTER HARDWARE AND SOFTWARE USED FOR PERFORMING CALCULATIONS.....	5
2.1 COMPUTER HARDWARE.....	5
2.2 COMPUTER SOFTWARE.....	5
3 FDTD MODELS.....	6
3.1 ANTENNA MODEL.....	6
3.2 KUSTER HOMOGENEOUS HEAD MODEL.....	7
3.2.1 <i>Nose of Model Centered Over Geometric Center of Patch Array</i>	8
3.2.2 <i>Nose of Model Centered Over Geometric Center of Lower Right Patch</i>	8
3.3 REMCOM HEAD AND SHOULDERS MODEL.....	8
3.4 INHOMOGENEOUS RECTANGULAR SLAB TORSO MODEL.....	9
4 ANTENNA FAR FIELD RADIATION PATTERN CALCULATIONS.....	21
5 ANTENNA NEAR FIELD CALCULATIONS.....	27
5.1 ANTENNA MODEL GEOMETRY.....	27
5.2 ELECTRIC FIELD CALCULATIONS AND MEASUREMENTS.....	28
5.3 ANTENNA MAGNETIC FIELD CALCULATIONS AND MEASUREMENTS.....	51
6 FDTD CALCULATION AND MEASUREMENTS OF SAR IN KUSTER HEAD AND SHOULDERS HOMOGENEOUS MODEL.....	71
6.1 ORIENTATION WITH TIP OF NOSE IN CONTACT WITH RADOME AND 9 MM BELOW CENTER OF FOUR PATCH ARRAY.....	71
6.2 ORIENTATION WITH TIP OF NOSE IN CONTACT WITH RADOME AND CENTERED OVER LOWER RIGHT PATCH.....	97
6.3 ORIENTATION WITH SIDE OF HEAD IN CONTACT WITH RADOME IN VARIOUS POSITIONS.....	107
7 FDTD CALCULATION OF SAR IN REMCOM HEAD AND SHOULDERS INHOMOGENEOUS MODEL.....	120
8 FDTD CALCULATION OF SAR IN INHOMOGENEOUS RECTANGULAR SLAB TORSO MODEL.....	138
8.1 EXPOSURE TO DOUBLE FEED ANTENNA.....	138
8.2 EXPOSURE TO SINGLE FEED ANTENNA.....	172
9 FDTD CALCULATION OF SAR IN HOMOGENEOUS RECTANGULAR SLAB TORSO MODEL.....	179
10 CONCLUSIONS.....	189
11 REFERENCES.....	190
APPENDIX A	
APPENDIX B	
APPENDIX C	

Executive Summary

This is a report on the evaluation of the AT&T Wireless Services Fixed Wireless RU Antenna in terms of its compliance with United States Federal Communications Commission (FCC)(1996) general population radio frequency (RF) maximum permitted human exposure limit (MPL). The report was completed according to the terms of a Services Agreement between AT&T Wireless Services (ATTWS) and Bioelectromagnetics Consulting (BEMC) signed on September 18, 1997.

BEMC completed the following tasks with results described in this report:

Performed theoretical calculations of the gain, radiation patterns, near fields and far fields of the AT&T RU antenna and compared the results with the FCC MPL and measurements of the values from other laboratories.

Performed theoretical calculations of the specific absorption rate (SAR) distributions in four models exposed to the AT&T RU antenna. The models consisted of the SPEAG homogeneous phantom human head also occasionally referred to in this report as the Kuster homogeneous head model, the REMCOM inhomogeneous phantom head, an inhomogeneous flat rectangular slab phantom (including skin, subcutaneous fat and muscle) and a homogeneous slab muscle model. The calculated SARs expressed in the form of tables, two dimensional color contour plots and line graphs were compared to the FCC and ANSI/IEEE (1992) MPLs and measurements of the values from other laboratories.

Assisted ATTWS in directing and verifying criteria such as methods, procedures, testing, models, results and other related events in the commissioning of two outside laboratories for making experimental measurements that validated and verified the theoretical calculations and comparison of results with the FCC MPLs.

The selected laboratories included:

Schmid & Partner, Engineering AG (SPEAG), Staffelstrasse 8, 8045 Zurich, Switzerland, with Dr. Neils Kuster as project director, who was responsible for carrying out measurements of the near and far fields from the RU antenna and SAR distribution in homogeneous phantom head and a flat rectangular tissue models exposed to the antenna fields.

SARTest Ltd., Oakfield Laboratories, Cudworth Lane, Newdigate, Surrey RH5 5DR. UK., with M.I. Manning as project director, who was responsible for carrying out measurements of the near and far fields from the AT&T RU antenna and SAR distribution in a heterogeneous phantom head model and a flat heterogeneous rectangular tissue model exposed to the antenna fields.

During the week of November 19 - 26, 1998, Keith Peavler of ATTWS and Arthur W. Guy of BEMC traveled to the SPEAG and SARTest laboratories to review the facilities and formulate agreements on the types of measurements that would be done.

BEMC, SPEAG and SARTest, each were provided with a model of the antenna which consisted of a 4 patch antenna array fed from a stripline network connected to two coaxial cable input power connectors. The patch antenna array and stripline network was backed by a ground plane designed to be bolted to a mounting framework covered by a plastic radome. The gain of the antenna as provided by the manufacturer was stated to be 15.03 dBi when each coaxial input connector is fed with in-phase equal power. For this analysis the total input power at a frequency of 1.92 GHz split equally between coaxial feed connectors was assumed to be 19.0 dBm or 79.62 mW, resulting in an effective radiated power as compared to an isotropic radiator (e.i.r.p.) of 2.54 watts (about 27% or 1.04 dB higher than the expected 2 watt e.i.r.p. level operational level of the antenna). Prior to the completion of this report, AT&T Wireless Services Engineers decided to operate the RU antenna with the full power to one feed (lower) with the other feed used for receiving only. The results from the analysis of the antenna powered with two feeds were validated as being the same for the antenna powered with one feed by performing an analysis of the SAR distributions in the inhomogeneous slab model when exposed to the latter antenna. The difference in the maximum SARs from the two analyses was less than 0.23 dB.

SPEAG completed their work and provided a report in August, 1998 which is attached to this report as Appendix A. SARTest completed their work on near electric fields and submitted a report on the measurements in July, 1998 which is included in this report as Appendix B. SARTest submitted a report on their SAR measurements in exposed homogeneous and inhomogeneous slab and human head phantoms in September 1998, which is included in this report as Appendix C.

The main body of this report deals with the theoretical calculations but where appropriate the results are compared to the measurements made by SPEAG and SARTest appearing in Appendices A, B and C.

The finite difference time domain (FDTD) technique was used to calculate the near and far fields and induced SAR patterns in exposed tissues from the antenna. The FDTD technique is currently the most popular theoretical method of choice for analyzing the safety and compliance of wireless technology devices with human RF exposure MPLs. There was perfect agreement between the calculated and manufacturer's measured antenna radiation patterns and gain and near perfect (within 0.27 dB) agreement between the calculated and the corresponding SPEAG measurements. The calculated near electric and magnetic fields agreed (within 0.22 dB) with the SPEAG measured E and H fields. There was agreement (within 1.8 dB at less than 40 mm and 0.8 dB at more than 40-mm distance from the ground plane) between the SARTest measurements of E fields and the corresponding calculations. Though the difference between calculated and the SARTest measurement results are large, they are within the +/- 2-dB accuracy estimated for their measurement system. With the exception of the maximum SARTest measurements (0.9 to 1.5 dB above the MPL) of the E-field at the surface of the radome all other calculated and measured near field strengths at and outside of the antenna radome were below the FCC MPL (-0.4 dB at radome and -6.4dB at 5 cm from radome).

One-gram average SAR levels rather than near field measurements must be used to determine compliance with the FCC MPL at distances less than 20 cm from the antenna.

The maximum calculated and measured SAR for all models exposed while in contact with the radome were below the FCC MPL for the normal antenna operating e.i.r.p. of 2 watts. The values compared to the MPL ranged from the worst case of -1.23 dB for the tip of the nose of the SPEAG homogeneous head model oriented at the center of the antenna patch with the highest fields to -14.7 dB for the REMCOM inhomogeneous head model exposed with the tip of the nose oriented at 9 to 10-mm below the center of the antenna array. For all other models and exposure positions the maximum SARs varied from -6.23 dB to -11.9 dB below the FCC MPL. Thus, it may be concluded from the calculations and measurements discussed in this report that anywhere outside of the radome, continuous human exposure to the AT&T RU antenna would be in compliance with the FCC MPL for continuous exposure.

1 Introduction

The FDTD method used for the SAR calculations presented in this report directly solves Maxwell's equations in the time domain. The concept was first reported by Yee, (1966) at a time when computers were too limited in speed and memory to put it into practical use. With the availability of improved computers, it was put to use for the first time nearly a decade later by Taflove and Brodwin (1975a) for solving scattered fields from a dielectric cylinder. This was followed the same year by the first application of the FDTD to calculate the induced fields and temperature in biological media (the human eye) exposed to microwave radiation by Taflove and Brodwin (1975b). With Taflove's, (1980, 1988) continued use of the FDTD as an important analytical tool for solving a multitude of different electromagnetic problems, many investigators began to use it (Lau et al., 1986), (Sullivan et al., 1987, 1988) for modeling biological systems exposed to RF fields.

The FDTD method has recently become the tool of choice for characterization of the SAR patterns in the human head exposed to cellular and PCS telephones. Gandhi (1996) was one of the first investigators to formulate an FDTD model for calculating the SAR from exposure to RF fields from cellular telephones. His model like those of many other investigators following him is based on Magnetic Resonance Imager (MRI) scans of the body of a human volunteer, obtained every 3 mm from the top of the head to the feet, which providing a resolution of about 2 mm per pixel for each body cross-sectional slice. Each of the close to 30 identified tissues in the MRI scan, was coded with numbers referring to its unique dielectric properties. The FDTD technique utilizes as input, the construction details including the RF radiating structure and excitation parameters of the telephone as well as the characteristics and dielectric properties of the exposed model of the body. This information is then fed into a computer and Maxwell's equations are solved using the FDTD method. The result is a detailed 3-dimensional pattern of the electric and magnetic fields in the air or in the tissue, which may easily be converted to SAR and visualized by standard graphical visualization software.

There has now been a flood of new papers reporting the use of the FDTD method in the applications of RF energy to medicine and biology as well to studies of RF biological effects. A number of new such publications appear in a special issue of the IEEE Transactions on Microwave Theory and Techniques on Medical Application and Biological Effects of RF/Microwaves (Rosen and Vander Vorst, editors, 1996).

2 Computer Hardware and Software Used for Performing Calculations

2.1 Computer Hardware

The theoretical calculations were performed on a 275 MHz, DEC Alpha 3000-900 Workstation equipped with 1 Gbyte of RAM and 10 Gbytes of hard disk space. The resulting calculated data and graphs were moved by local ethernet to a Micron 180 MHz PC for final processing and integration with the report. The final report and figures were printed on a Tektronix 560 color laser printer. A Summagraphics SummaSketch III, 12x18 inch, 0.223 mm resolution graphics tablet was used to digitize the configuration of the RU antenna for introduction into the FDTD model space.

2.2 Computer Software

An FDTD software package commercially available from REMCOM Corporation [State College, PA], called XFDTD (version 404) was used to carry out all of the SAR calculations discussed in this report. All of the calculations of SAR conducted with the XFDTD software utilized the default timestep interval of 1.926 ps and total of 4000 time steps. The XFDTD software calculates the SAR based on the 3 electric field components corresponding to the 3 edges intersecting at the corner nearest the origin of each FDTD cell. A shareware program called xv was used to grab the model, field and SAR distribution images from the workstation monitor screen and convert them into GIF files for storage or transfer to a PC for processing by other imaging software.

For validation purposes, a limited number of XFDTD SAR calculations were done previous to the time of this reported work and compared with theoretical values obtained from the Mie scattering theory computer code developed by Ho and Guy (1975) for a sphere exposed to a plane wave. For example one validation involved a 1.4-cm diameter model sphere exposed to a 3.0 GHz plane wave. The sphere was centered in a 0.4-mm cubical mesh of 75x75x75 cells with Liao et al. (1984) type perfectly matched layer (PML) outer boundaries. A total of 3000, 0.77 ps wide time steps were used for the calculations. The calculated SAR distributions at 3 GHz agreed with the Mie theory derived values to within 3.7% for the maximum SAR and 0.71% for the whole-sphere-average SAR.

3 FDTD Models

3.1 Antenna Model

The RU antenna was completely disassembled and the dimensions of each part were carefully measured with Fowler Ultra-Cal model III digital calipers. The surface of a SummaSketch III graphics tablet was covered with a 11x17-inch sheet of mm scale graphics paper taped to its surface. The outside periphery of the antenna ground plane and the polygonal shaped patch array and associated stripline circuitry were each traced to the surface of the graph paper with an accuracy of +/- 0.5-mm. The graphics tablet stylist was then used to digitize the outline of the ground plane and the patch array/stripline combination and download them to computer files.

A Fortran program was written and run to convert the antenna outline data files into the XFDTD program graphical image files. The graphical users interface (GUI) feature of the XFDTD program was then used to assemble and convert the antenna ground plane and patch array/stripline outlines into solid 1mm thick sheet metal solid objects within a 51x306x366, cell mesh of 1x1x1-mm cubical cells. The objects were graphically reassembled and the other antenna parts, including feed points were added via the GUI and a 1 volt, zero phase source in series with a 50 ohm resistance was applied at each feed point.

Since the cell mesh containing the antenna model contains 5.7 million cells and each cell requires 30 bytes of RAM, a total of 171 Mbytes in addition to that required by the XFDTD program and operating system of computer RAM is required to calculate the fields within the selected FDTD space. Thus if the 1-mm cell size FDTD space is increased to allow the calculation of near fields out to a desired half meter distance from the antenna to insure continuity to the far field region, the 1 Gbyte RAM limit of the computer would be greatly exceeded. Fortunately to handle this type of problem the XFDTD software allows three different mesh sizes to be used in the same FDTD space. The proper characterization of the antenna requires the relatively fine grid of 1-mm size cells. However at increasing distances from the antenna where less resolution is required to characterize the fields, a courser mesh may be used. The memory size problem was taken care of by first formulating what is called a main mesh or grid, using a 210x210x212 cell mesh of 3x3x3-mm cubical cells. Another mesh called a local mesh consisting of the 1x1x1-mm-cubical cells containing the antenna was placed within the main mesh. Three views of the FDTD space geometry, grabbed directly from the GUI of the XFDTD are shown in Figures 3.1, 3.2 and 3.3.

Figure 3.1 illustrates an x-z plane cross-sectional view of the FDTD meshes containing the antenna. For this model the long axis of the antenna ground plane was oriented vertically along the z-axis, the minor axis of the ground plane was oriented horizontally along the y-axis and the x axis was oriented perpendicular to the antenna ground plane. The locations where two dimensional field distributions were selected for plotting from the calculated data are denoted by

black lines identified by alphabetical letters from A through Q. The distances of the selected planes from the origin of the coordinate system at the lower right corner of the main mesh are given in terms of number of 3-mm cells at the top of the graph of the main mesh. These distances are in turn related to distances from the antenna ground plane and radome in the lower half of the main mesh. Black lines also mark the location of the radome and the location of the selected field distribution (40-mm from the ground plane) where detailed comparisons were made with measured field distributions in Appendices A and B. The line marked current ANSI marks the closest distance (within the nearest 3-mm increment) that the ANSI/IEEE and FCC MPL allows field measurements to be made for compliance and the distance within which SAR measurements are required to determine compliance if the radiated power exceeds the e.i.r.p. allowed for certain low power emitters. The line marked new ANSI is the new recently IEEE Safety Standard Coordinating Committee (SCC-28) approved closest allowed distance for field measurements to be made to determine compliance.

Figure 3.2 illustrates a section in the x-y plane and Figure 3.3 illustrates a section in the y-z plane through the active patches and associated stripline circuitry of the FDTD meshes showing similar information as discussed above.

3.2 Kuster Homogeneous Head Model

The FDTD model of the Kuster experimental phantom head was derived from a file containing data from MRI scans of the SPEAG head and upper torso human model. Dr. Kenneth Foster of the University of Pennsylvania made the scans of the phantom, consisting of 2 to 4-mm thick Plexiglas shell filled with liquid. The shape of the shell was equivalent to that of the surface of one half of a human body separated at the sagittal plane. A Fortran program was written to convert the scan data into the format used by the XFDTD program. The GUI of the XFDTD was then used to duplicate the half phantom in a 270x306x366-cell mesh of 1x1x1-mm cells containing the antenna. The duplicate was then inverted and joined with original half and the resulting model was truncated it to produce a complete head and shoulders model in contact with the radome of the antenna within the mesh. The nose of the model was oriented with the tip in contact with the antenna radome and centered 9-mm below the geometric center of the four-patch array for one case and centered over the lower right patch for the other case. The latter proved to result in the highest SAR in the exposed nose of the model. A dielectric constant of 2.54 was assigned to the Plexiglas shell and the relative permittivity and conductivity of the liquid used to simulate the brain tissue in the experimental model were assigned values of 41.0 and 1.69 S/m, respectively. Though the dielectric properties for the simulated brain were published by SPEAG for 1.8 GHz rather than 1.92 GHz, they were the closest values available and were used at the time the model was analyzed.

3.2.1 Nose of Model Centered Over Geometric Center of Patch Array

Figure 3.4 illustrates the x-z section through the tip of the nose of the head and shoulders model at slice 154 of the FDTD mesh. Part of the back of the head and shoulders of the model had to be truncated to keep the size of the FDTD space within the 1 Gbyte RAM limit. The locations where two dimensional SAR and 1 gram average SAR distributions were selected from the calculated data are denoted by black lines identified by alphabetical letters from A through K. Figure 3.5 illustrates the x-y section of the model at slice 193 through the nose of the model. Locations of additional sections L through N where SAR and 1 gram average SAR distributions were selected are shown in the figure.

3.2.2 Nose of Model Centered Over Geometric Center of Lower Right Patch

Figure 3.6 illustrates the x-z section through the tip of the nose of the head and shoulders model at slice 228 of the FDTD mesh at the center of the lower right patch. Part of the back and sides of the head and shoulders of the model had to be truncated to keep the size of the FDTD space within the 1 Gbyte RAM limit. The locations where two dimensional SAR and 1 gram average SAR distributions were selected from the calculated data are denoted by black lines identified by alphabetical letters from A through U. Figure 3.7 illustrates the x-y section of the model at slice 126 through the nose of the model. Locations of additional sections V through X where SAR and 1 gram average SAR distributions were selected are shown in the figure.

3.3 REMCOM Head and Shoulders Model

The REMCOM XFDTD software used by BEMC was optionally supplied with a phantom man file based on the “visible man” model derived from a project under the direction of the National Library of Medicine. The original file is based on taking thin slices successively along a plane perpendicular to the long axis of a frozen deceased human and successively photographing the freshly cut surfaces of the remaining portion of the body. Information on the project is available on the Internet at <http://www.nnlm.nlm.nih.gov/sar/curr/95n6/nlmunvei.html>. REMCOM modified the file by thinning out the slices and adding the dielectric properties for each of the major tissues, resulting in a three dimensional FDTD meshed model of approximately 861500 cells (voxels) of 5x5x5 mm in size. A head and shoulders model meshed to a voxel size of 3x3x3 mm was also supplied. The cell size of the latter model used in this analysis was too large to obtain the desired SAR spatial resolution of 1-mm so a command feature of the XFDTD was used to decrease the cell size down by a factor of three yielding a head and shoulders model that was used to replace the SPEAG head model in the 270x306x366, 1-mm voxel space containing the antenna. Of course the reduction doesn't increase the resolution of the tissue structure but does improve the spatial resolution of the calculated SAR distribution and allows the model to occupy the same 1-mm mesh containing the antenna. Gabriel's (1996) equations were used to determine the

respective relative permittivities and the conductivities at 1.92 GHz for bone, 11.7 and 0.296 S/m; brain (white matter), 36.84 and 0.9662 S/m; cartilage, 39.94, 1.367 S/m; eye, 68.51, 2.105 S/m; muscle, 53.39, 1.408 S/m; and skin, 43.65, 1.293 S/m.

Figures 3.8 and 3.9 respectively illustrate sections of the model in the x-z plane at slice 154 and the x-y plane at slice 193 of the FDTD mesh (orthogonal planes through the tip of the nose). Sections of the model selected for illustrating SAR and 1 gram average SAR distributions are denoted alphabetically from A through N. The location of the tip of the nose was set to be the same as used for the Kuster head model in contact with the radome and 9-mm below the center of the patch array.

3.4 Inhomogeneous Rectangular Slab Torso Model

At the start of this analysis it was expected that highest SARs would occur for exposed body sections that could be in contact with and cover most of the radome such as the torso or the side of the head. It was decided that a slab model of the torso could represent the worst case scenario. Later, however, it was found as discussed in section 6.2 of this report that the highest SAR occurred when the Kuster head was exposed with the tip of the nose above the lower right patch of the AT&T RU antenna. A x-z plane section of the inhomogeneous model taken through the middle of the left patches of the array at slice 81 is shown in Figure 3.10 and an x-y section of the model taken through the middle of the lower patches of the array at slice 141 of the array is shown in Figure 3.11. The 152x277x366, 1-mm cell slab model consisted of an outside 2-mm thick layer of skin in contact with the antenna radome, a 11-mm thick layer of subcutaneous fat below the skin and the rest of the model below the subcutaneous fat consisting of a 139-mm thick layer of muscle. Sections of the model selected for illustrating SAR and 1 gram average SAR distributions are denoted by the black lines, labeled alphabetically from A through Q.

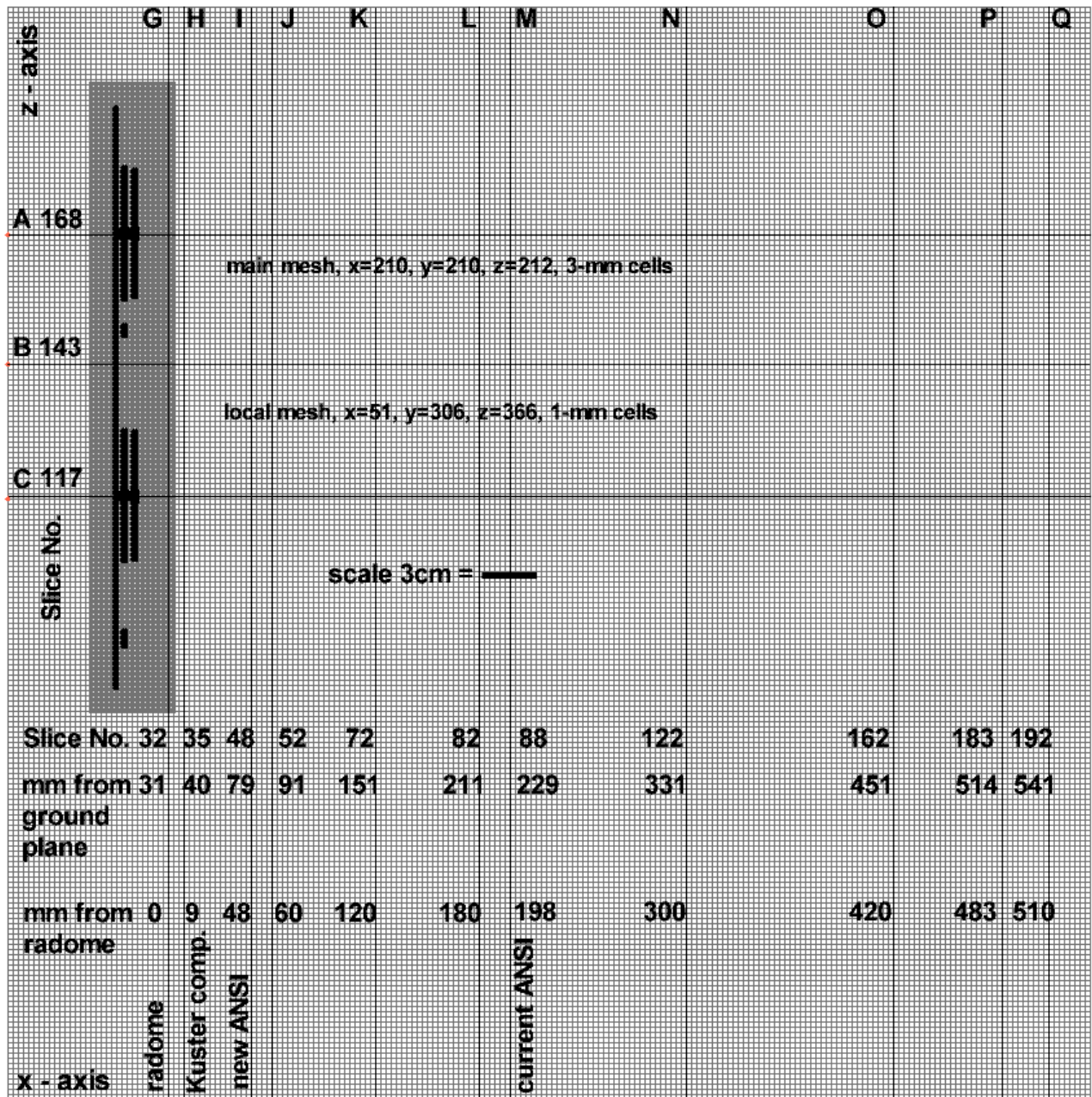


Figure 3.1. Graph showing x-z plane view, at y = slice 130, of AT&T Wireless Services RU antenna model within 1 mm local grid mesh which in turn is within 3- mm main grid mesh, showing locations of E-field and H-field plot planes selected from FDTD derived data (includes location of x and z axes, outermost surface of radome, data corroborated by Kuster's measurements, minimum distance from source allowed for measurements by both current and newly approved ANSI/IEEE standards).

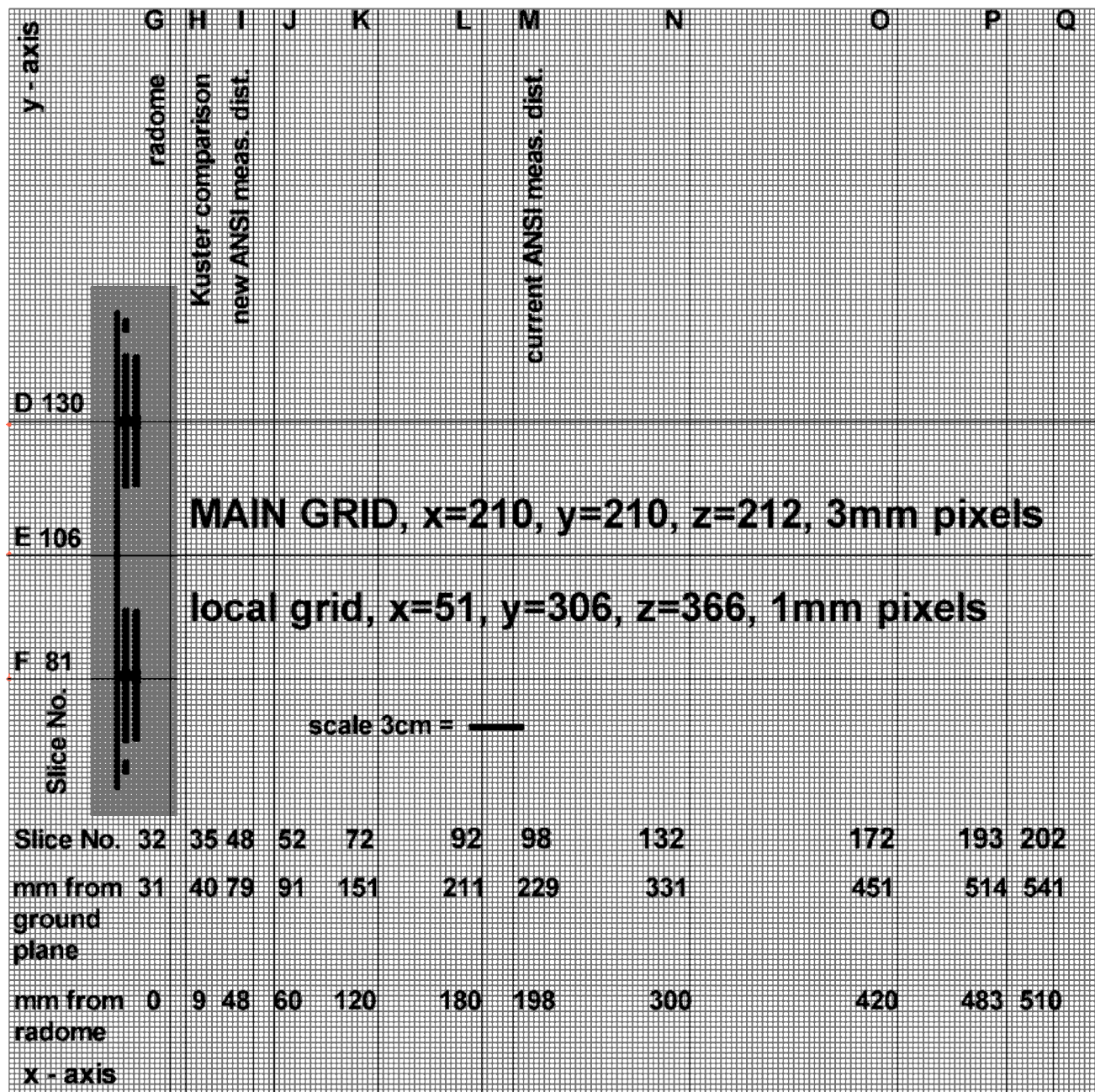


Figure 3.2. Graph showing x-y plane view, at z = slice117, of AT&T Wireless Services RU antenna model within 1 mm local grid mesh which in turn is within 3-mm main grid mesh, showing locations of E-field and H-field plot planes selected from FDTD derived data (includes location of x and y axes, outermost surface of radome, data corroborated by Kuster's measurements, minimum distance from source allowed for measurements by both current and newly approved ANSI/IEEE standards).

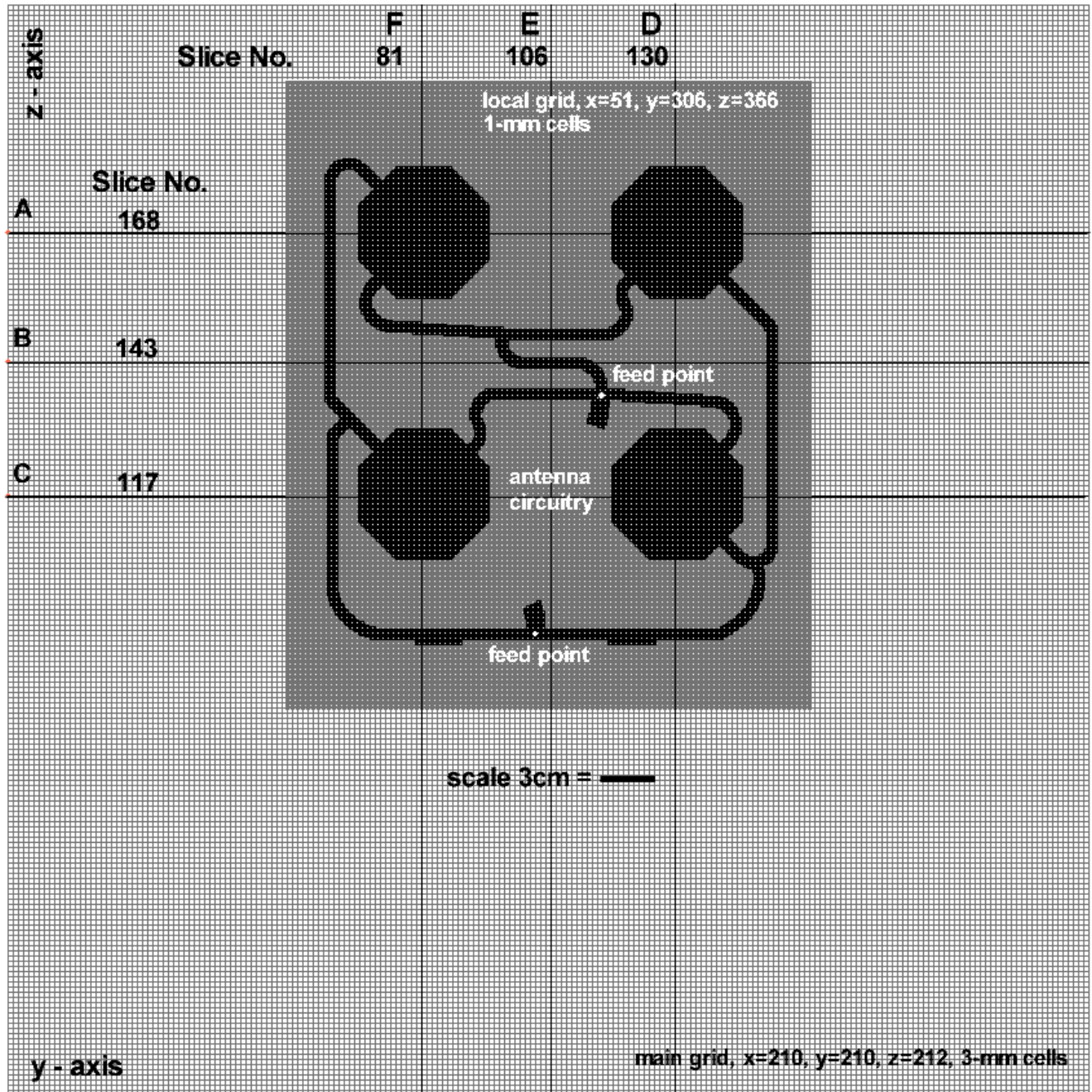


Figure 3.3. Graph showing y-z plane view, at x = slice 21, of AT&T Wireless Services RU antenna model within 1 mm local grid mesh which in turn is within 3 mm main grid mesh, showing locations of E-field and H-field plot planes selected from FDTD derived data (plane through antenna stripline circuitry contained within local grid which in turn is contained in main grid).

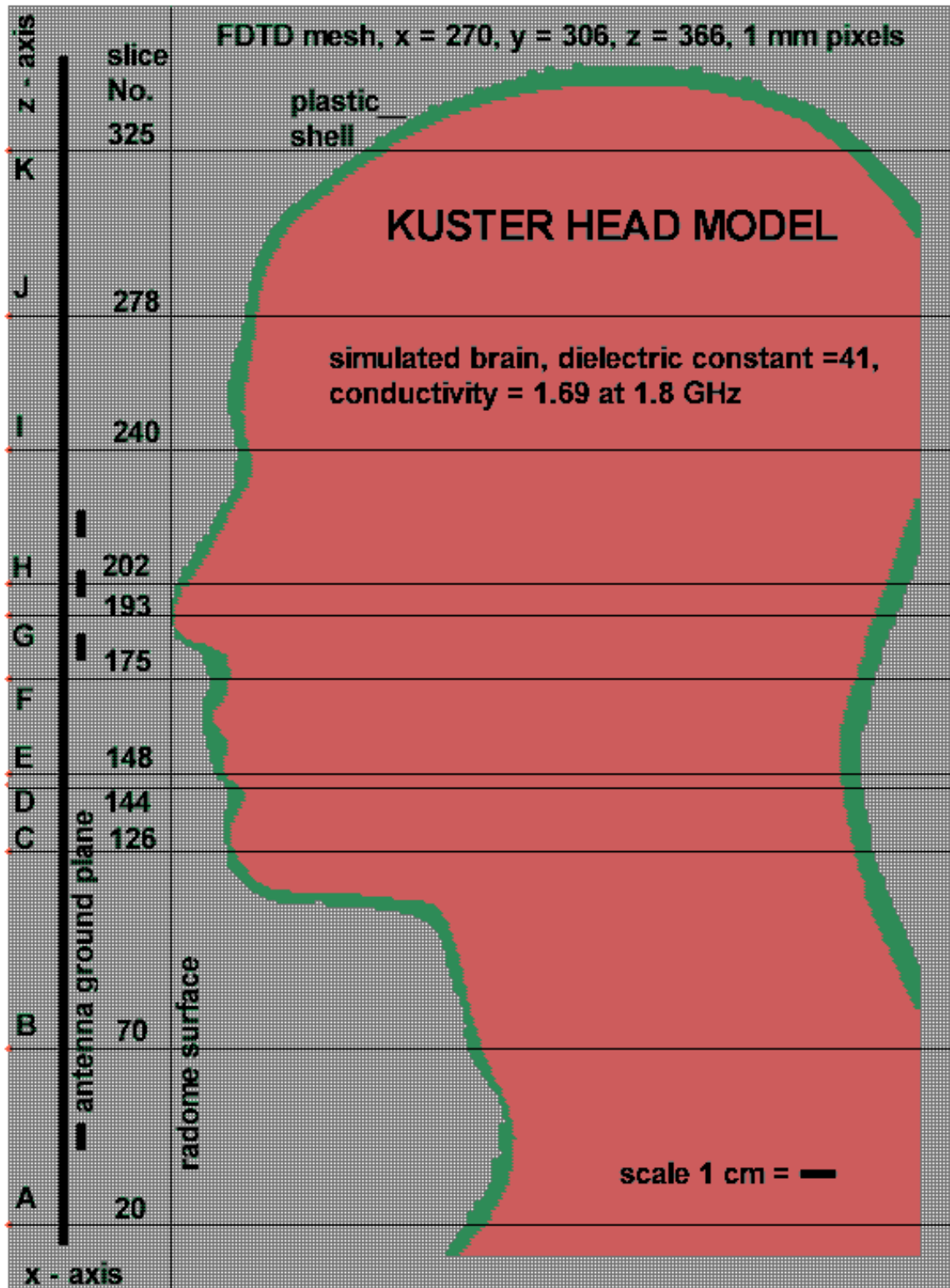


Figure 3.4. Graph showing x-z plane view at slice 154 of FDTD mesh containing Kuster head model exposed to AT&T RU antenna with tip of nose in contact with radome and centered 9-mm below middle of patch array (locations of selected x-y plane slices containing SAR data shown).

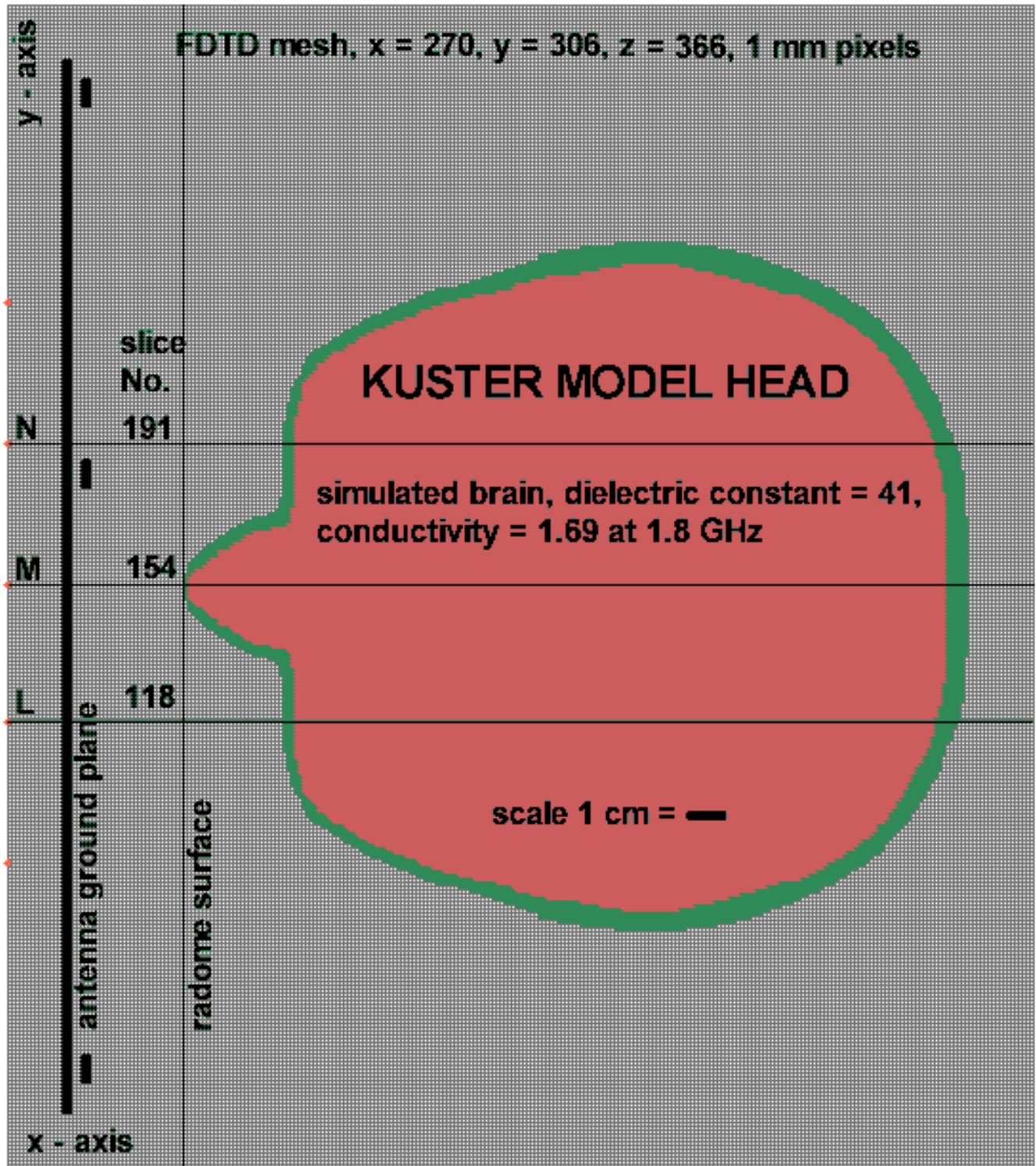


Figure 3.5. Graph showing x-y plane view at slice 193 of FDTD mesh containing Kuster head model exposed to AT&T RU antenna with tip of nose in contact with radome and centered 9-mm below middle of patch array (locations of selected x-z plane slices containing SAR data shown).

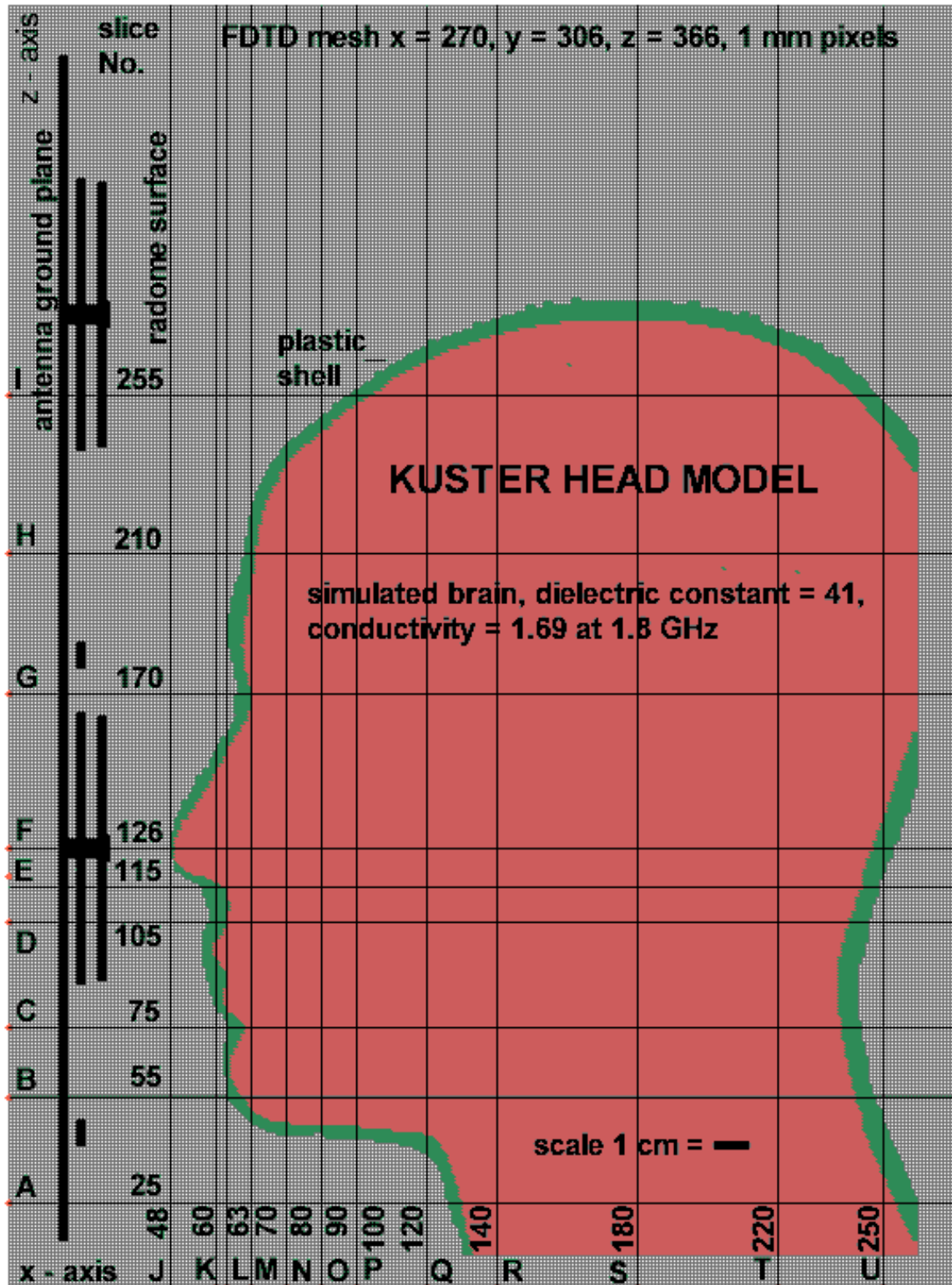


Figure 3.6. Graph showing x-z plane view at slice 228 of FDTD mesh containing Kuster head model exposed to AT&T RU antenna with tip of nose in contact with radome and centered over lower right patch (locations of selected x-y plane slices containing SAR data shown).

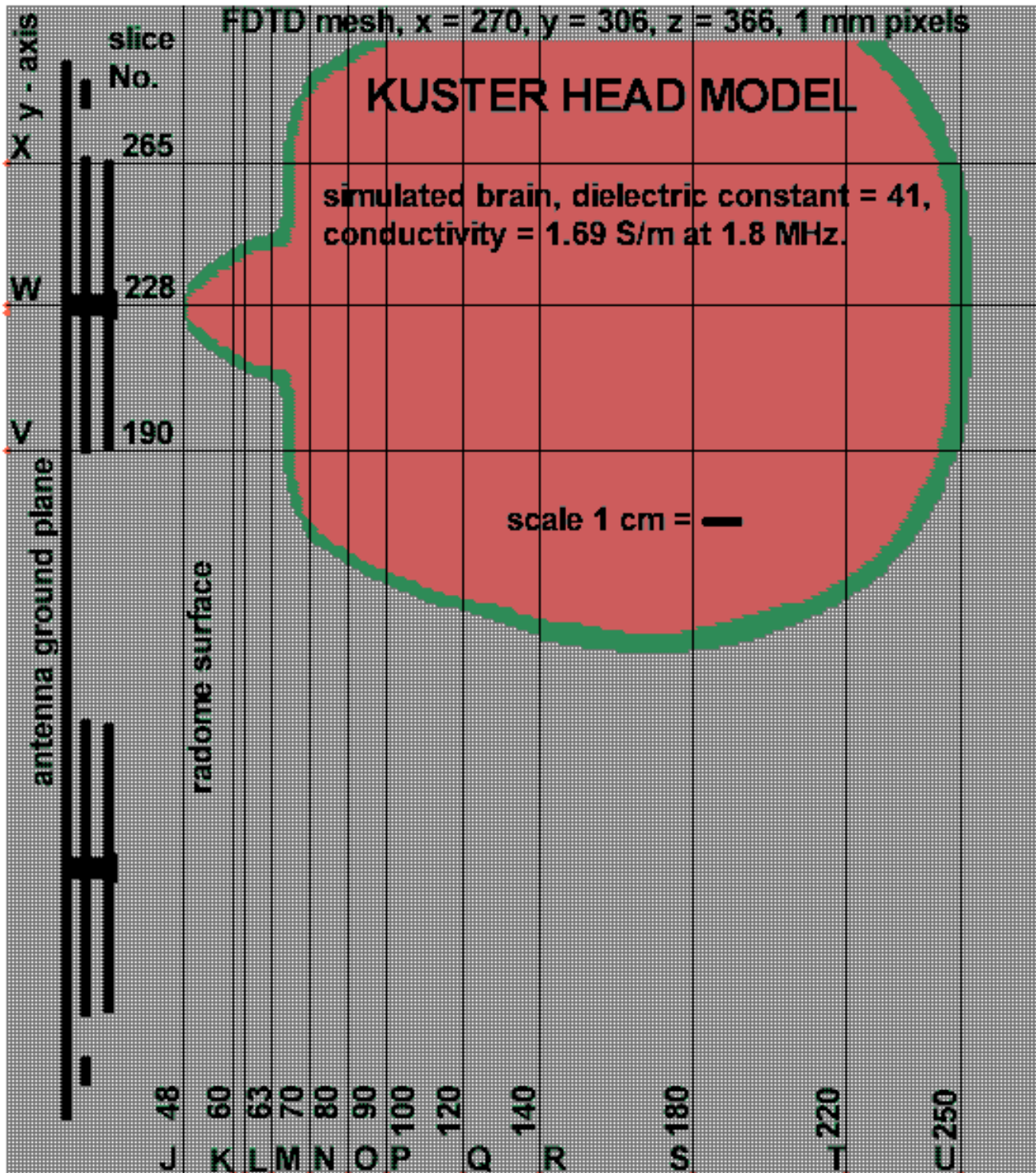


Figure 3.7. Graph showing x-y plane view at slice 126 of FDTD mesh containing Kuster head model exposed to AT&T RU antenna with nose in contact with radome and centered over lower right patch (locations of selected x-z and y-z plane slices containing SAR data shown).

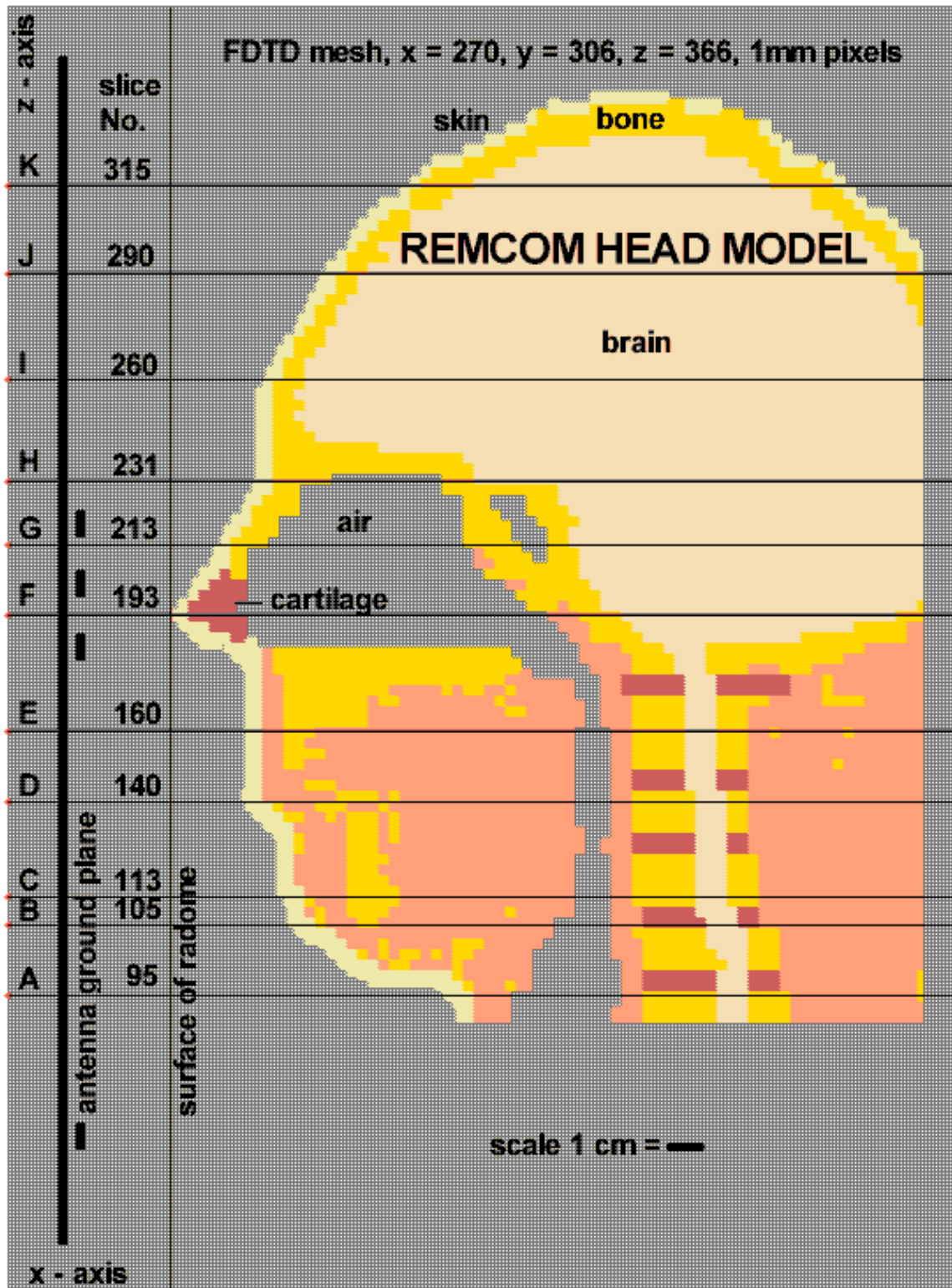


Figure 3.8. Graph showing x-z plane view at slice 154 of FDTD mesh containing REMCOM head model exposed to AT&T RU antenna with tip of nose in contact with radome and centered 9-mm below middle of patch array (locations of selected x-y plane slices containing SAR data shown).

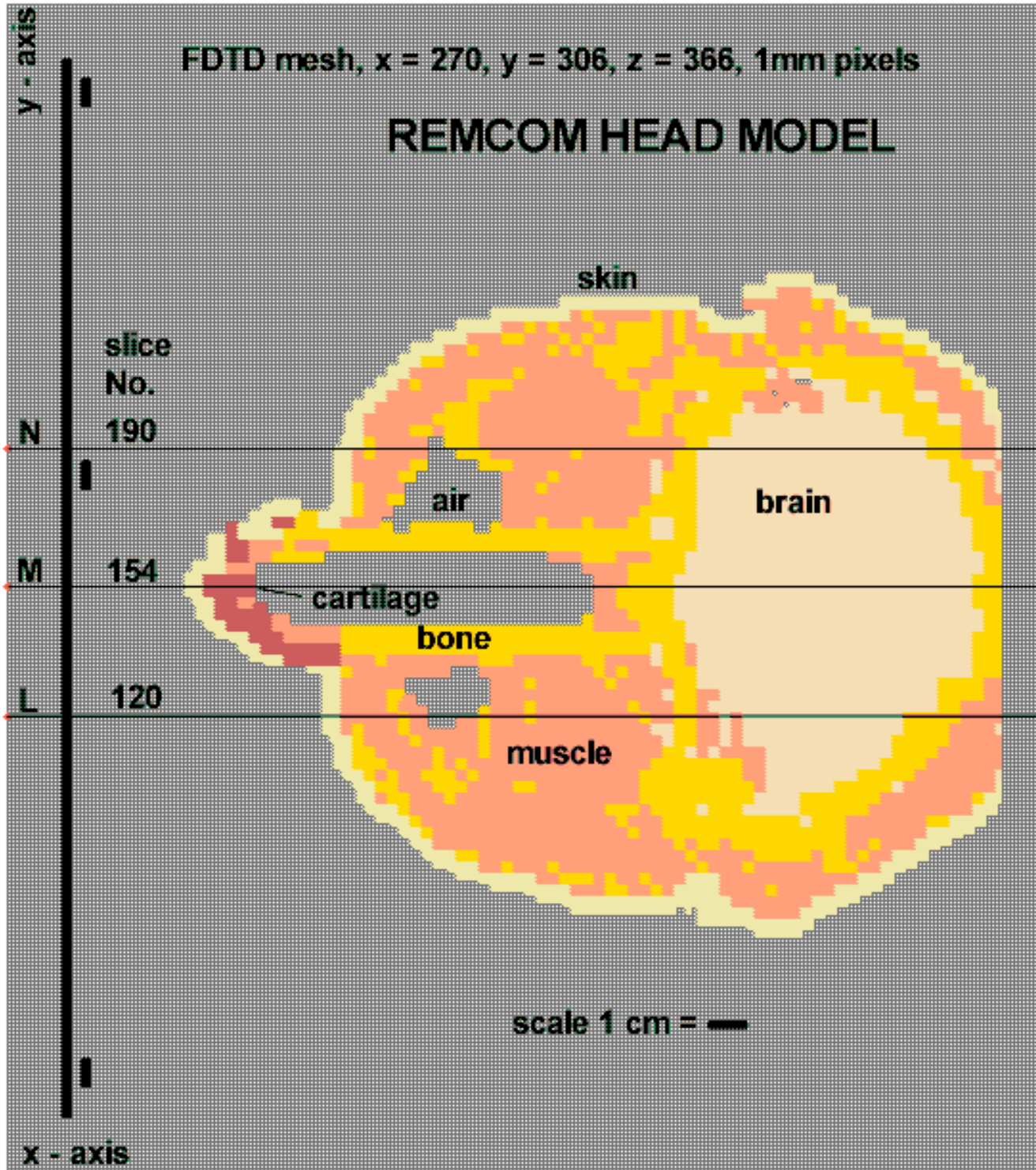


Figure 3.9. Graph showing x-y plane view at slice 193 of FDTD mesh containing REMCOM head model exposed to AT&T RU antenna with tip of nose in contact with radome and centered 9-mm below center of patch array (locations of selected x-z plane slices containing SAR data shown).

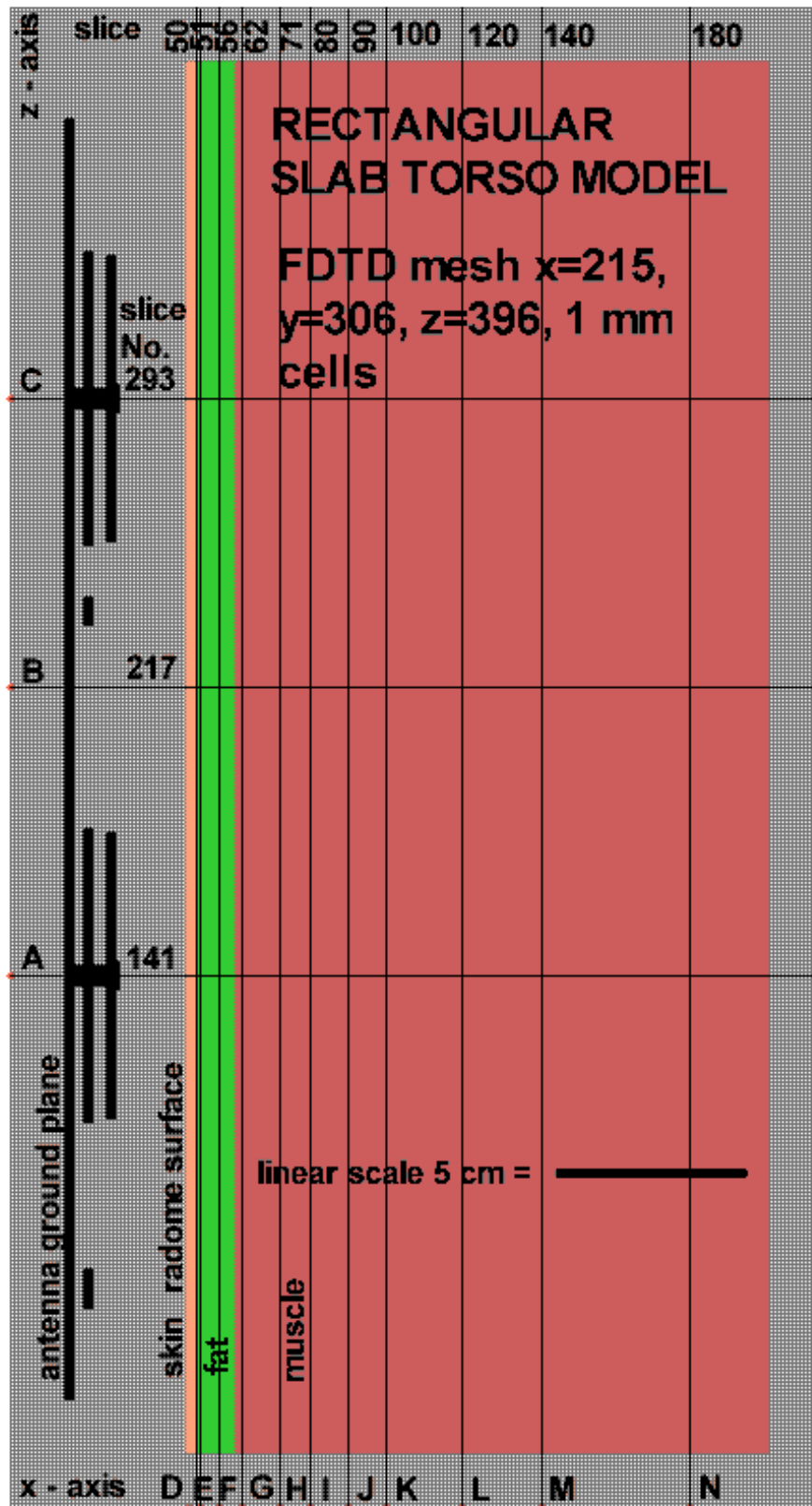


Figure 3.10. Graph showing x-z plane view at slice 81 of FDTD mesh containing slab torso model exposed to AT&T RU antenna (locations of selected x-y and y-z plane slices containing SAR data shown).

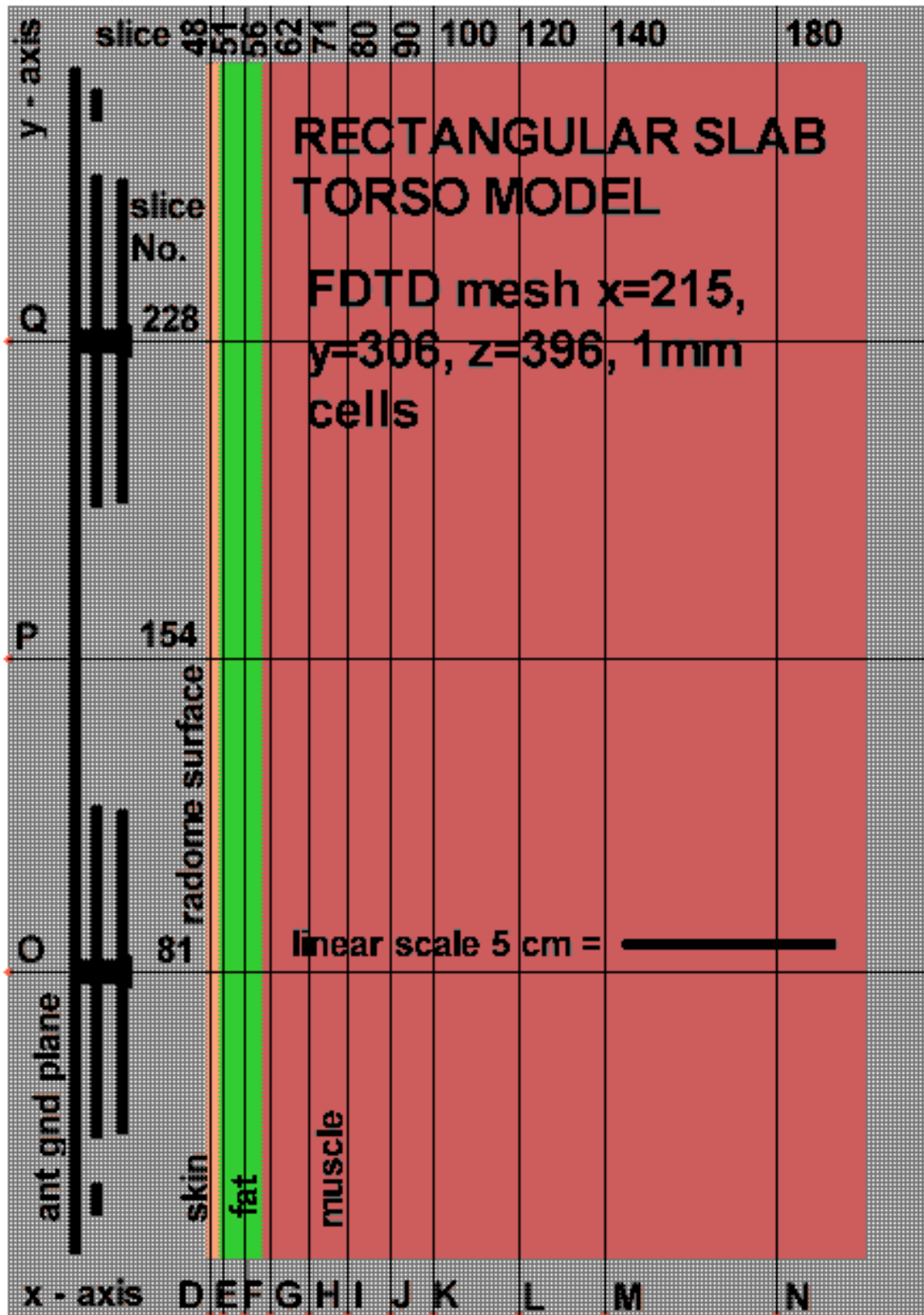


Figure 3.11. Graph showing x-y plane view at slice 141 of FDTD mesh containing slab torso model exposed to AT&T RU antenna (locations of selected x-z and y-z plane slices containing SAR data shown).

4 Antenna Far Field Radiation Pattern Calculations

patterns of the ATTWS RU antenna were calculated and compared to the patterns measured by the manufacturer and SPEAG. The XFDTD software can be used to calculate and save the complex steady state tangential fields on a closed surface surrounding the radiation structure. These tangential antenna fields can then be used by the XFDTD to obtain far zone radiation gain in any direction. To perform these calculations, the local mesh containing the antenna shown in Figures 3.1 through 3.3 was used to calculate the files containing the fields tangential to the closed surface surrounding the AT&T RU antenna. For these calculations the coordinate system was modified to better characterize the pattern with the position of the main beam corresponding to a reference angle of 0 degrees. This was done by orienting the z - axis perpendicular to the outside surface, the x - axis corresponding to the minor axis and the y - axis corresponding to the major axis of the antenna ground plane. The post-processing results of calculating the patterns are shown in Figures 4.1 through 4.4.

Figure 4.1 illustrates the horizontal radiation pattern along the x - z plane ($\phi = 0$) of the E_{ϕ} and E_{θ} electric field components for θ between -180 and 180 degrees. Figure 4.2 illustrates an expanded view for θ between -20 and 20 degrees of the same pattern. Figures 4.3 and 4.4 show similar vertical radiation patterns along the y - z plane ($\phi = 90$ degrees). The patterns indicate an antenna gain of 15.03 dBi for the vertical electric field component with the 30-degree wide main beam tilted approximately 2 degrees to the right and 2 degrees down. The maximum gain for the horizontal field component is shown to be approximately -8 dBi at -25 degrees. Both the vertical and horizontal patterns show symmetrical side lobes near plus and minus 50 degrees with a gain of 10 to 12 dB less than that of the main lobe. The calculated patterns appear to agree very well with the measured values provided by the manufacturer shown in Figure 4.5 and the values calculated by SPEAG shown in pages 11 through 20 in Appendix A.

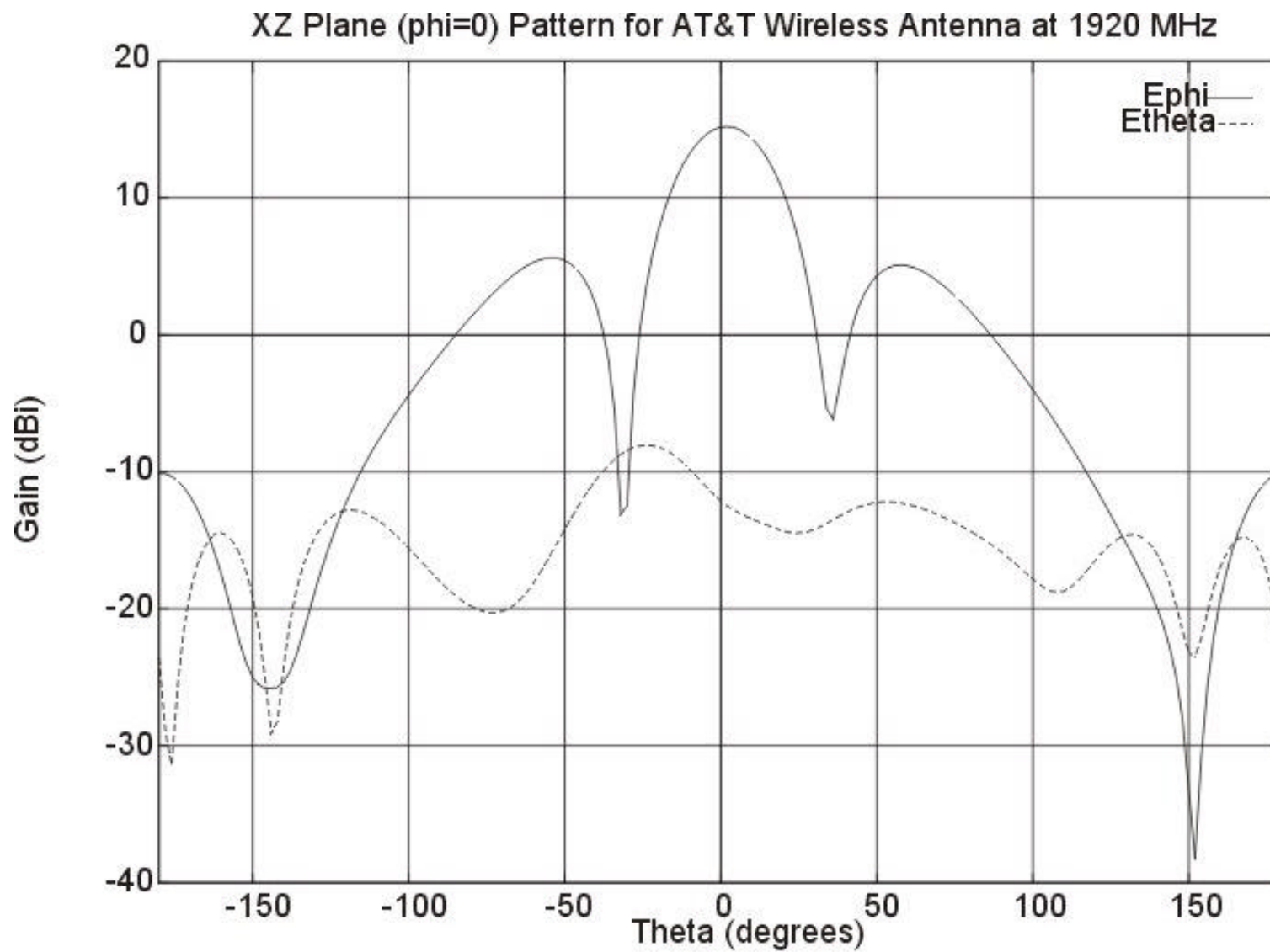


Figure 4.1. FDTD derived RU Antenna horizontal radiation pattern, theta = -180 to 180 degrees.

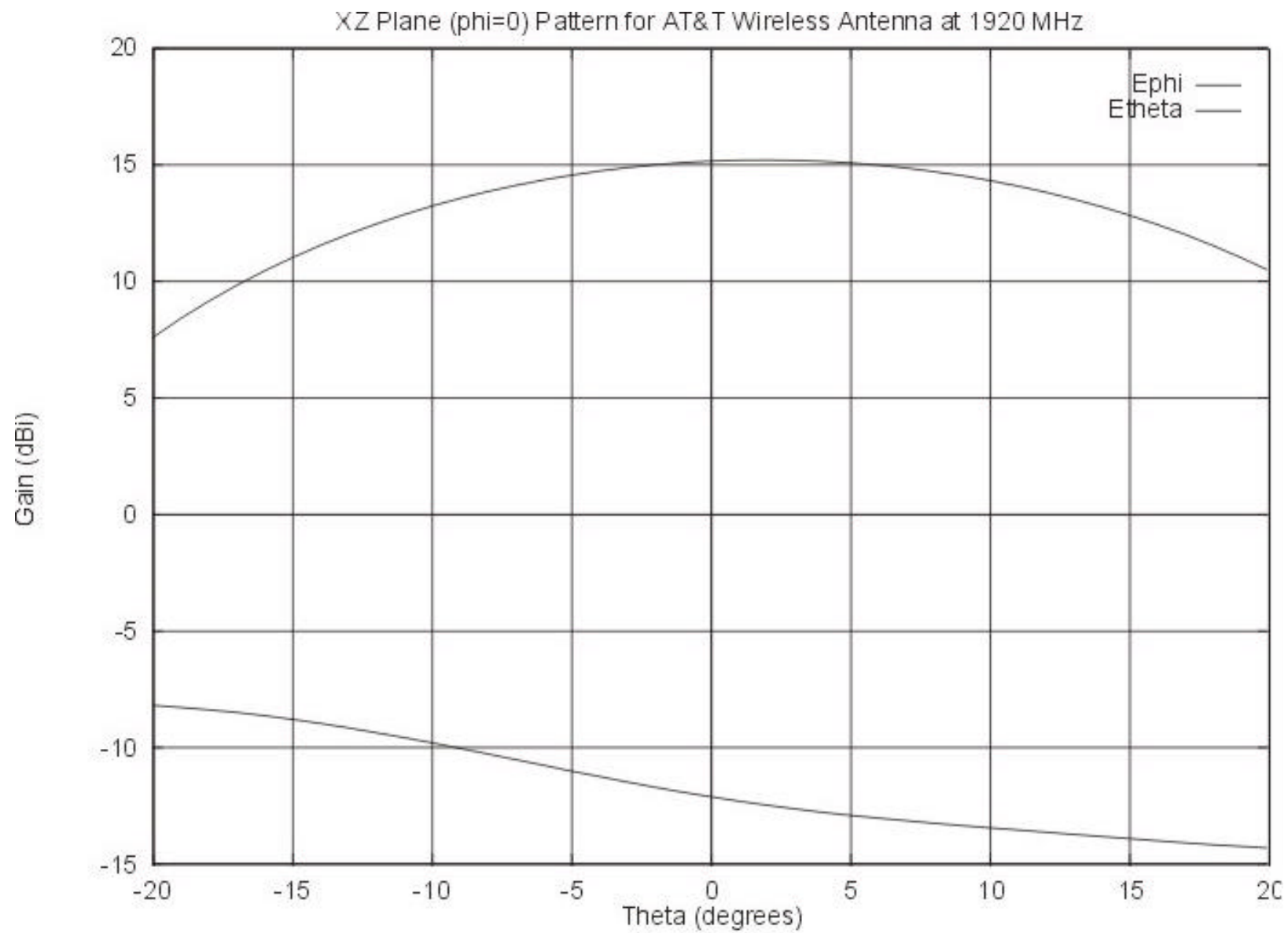


Figure 4.2. FDTD derived RU Antenna horizontal radiation pattern, theta = -20 to 20 degrees.

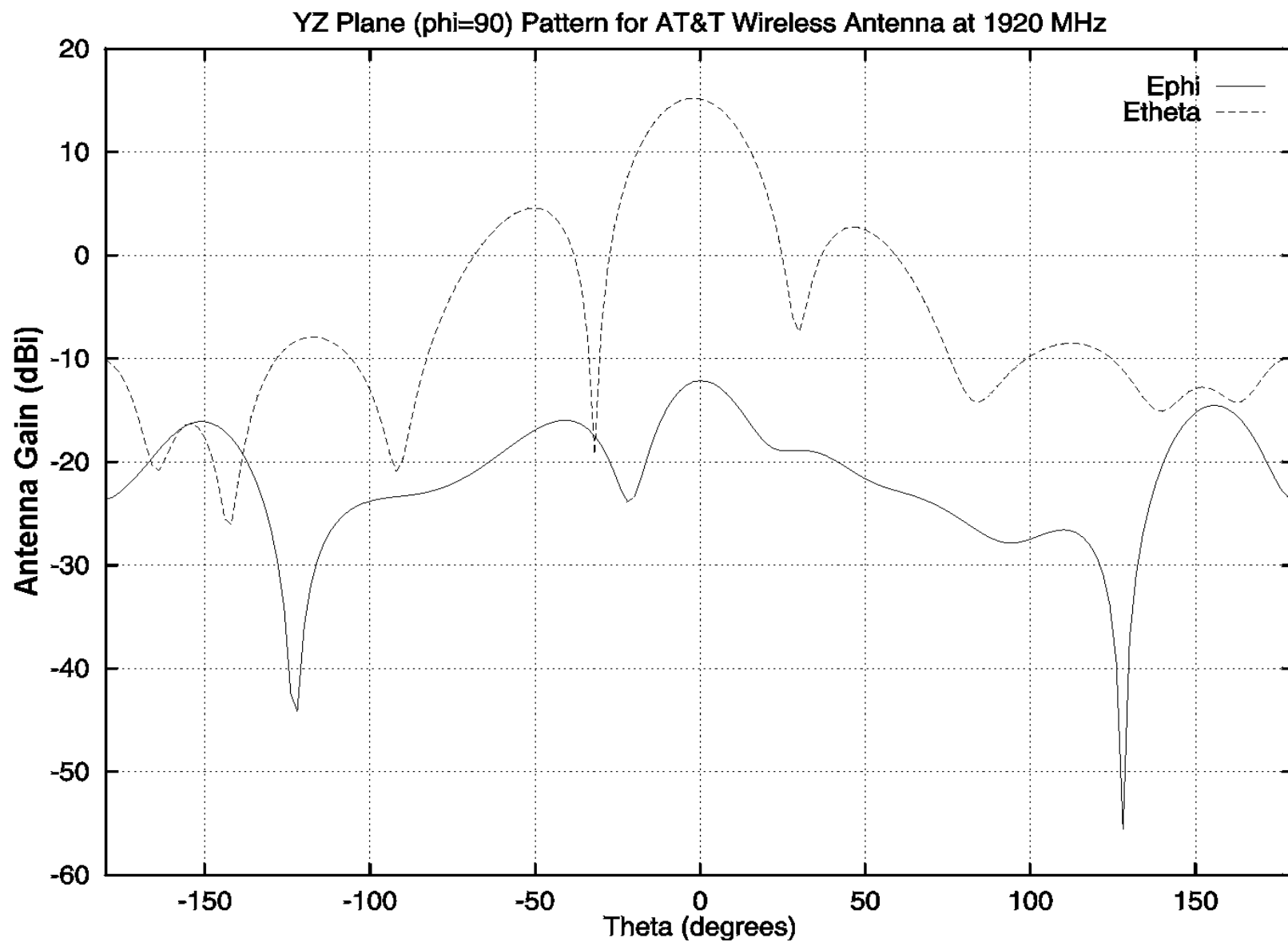


Figure 4.3. FDTD derived RU Antenna vertical radiation pattern, theta = -180 to 180 degrees

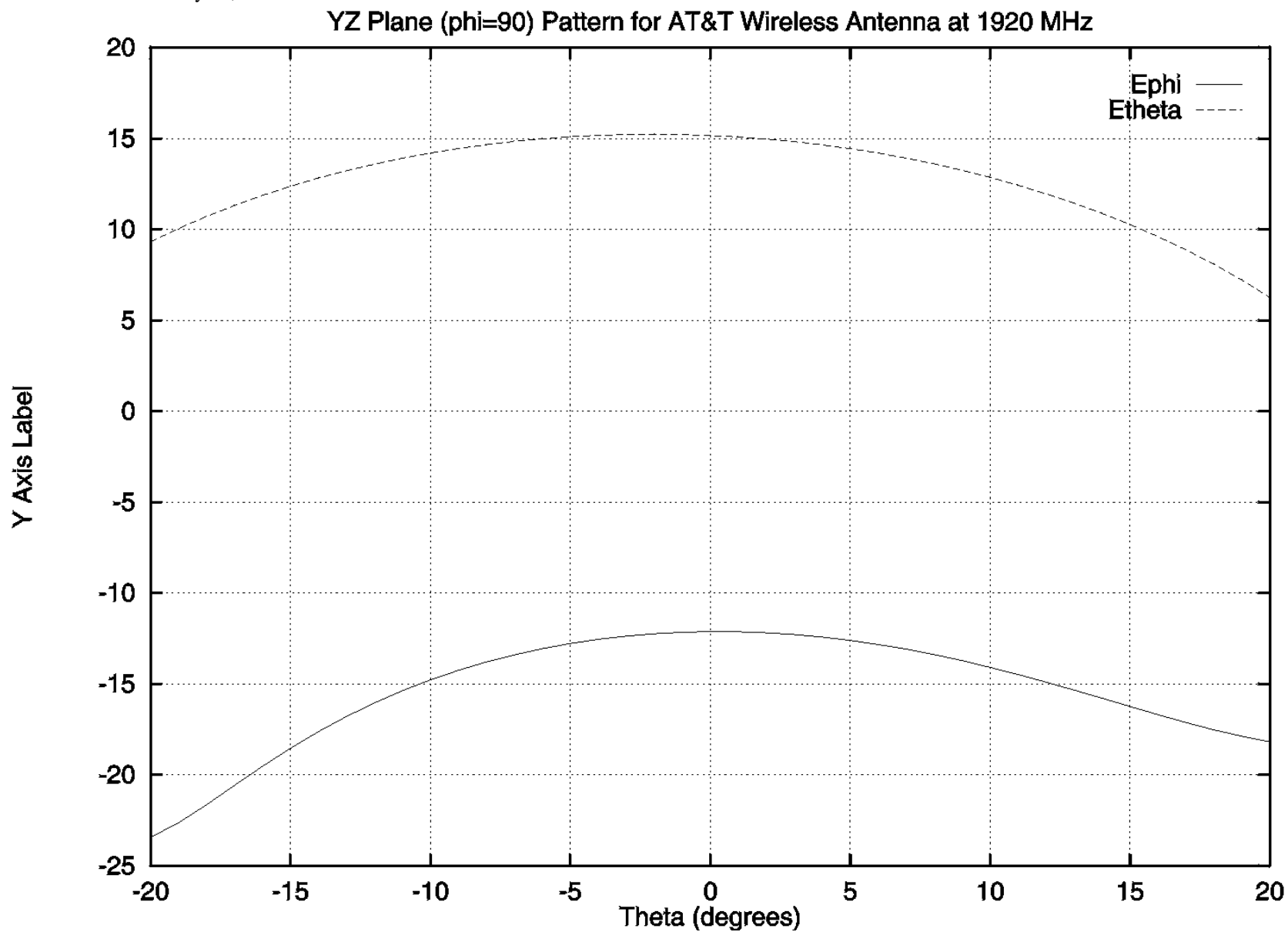


Figure 4.4. FDTD derived vertical radiation pattern, theta = -20 to 20 degrees.

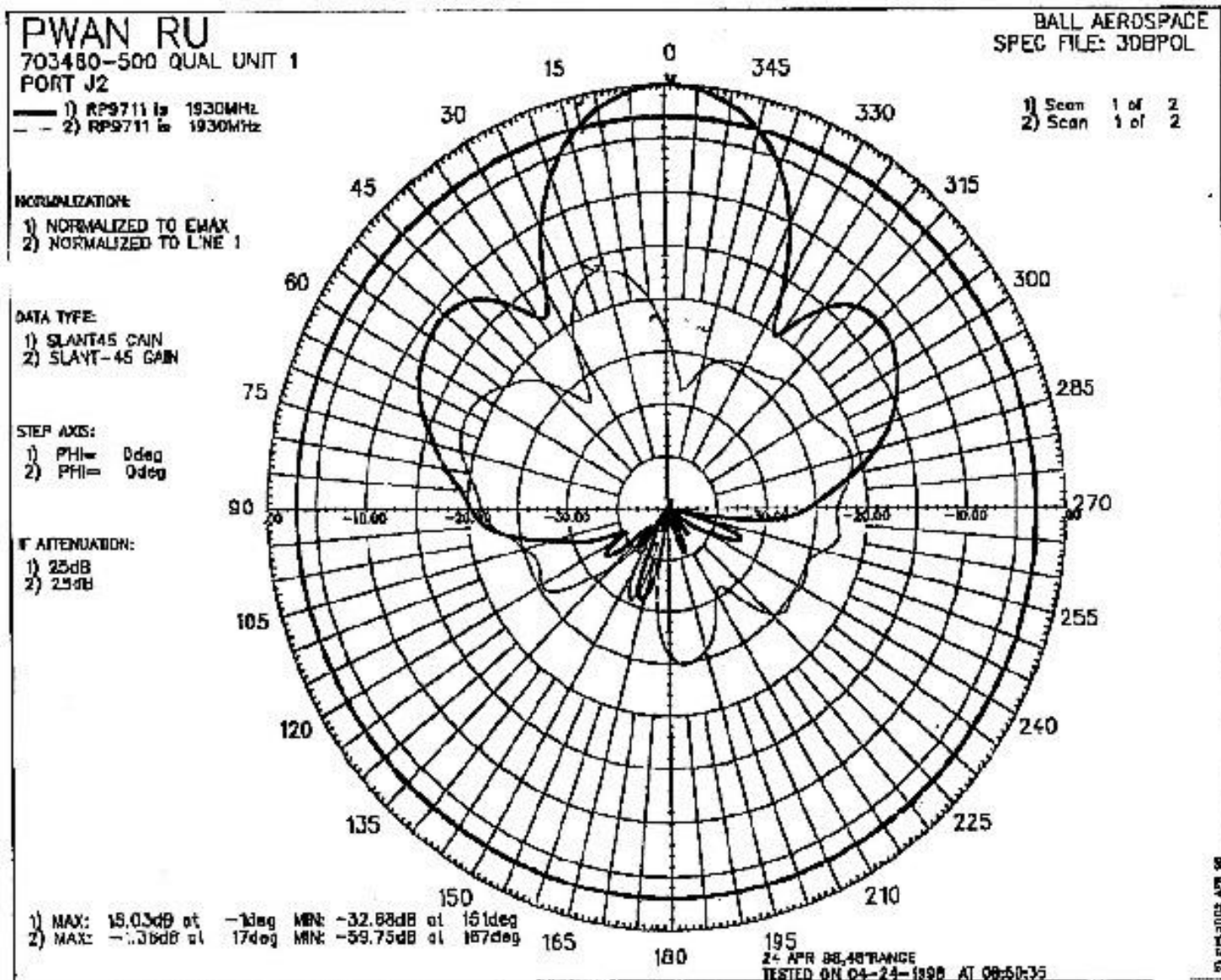


Figure 4.5. Manufacturer's supplied horizontal radiation pattern for AT&T RU Antenna.

5 Antenna Near Field Calculations

5.1 Antenna Model Geometry

Figures 3.1 through 3.3 illustrate the geometry of the near field computer FDTD model as it is meshed in a local grid of $366 \times 306 \times 51 = 5.71$ million cubical $1\text{mm} \times 1\text{mm} \times 1\text{mm}$ cells which in turn is contained in the main grid of $210 \times 210 \times 212 = 98.4$ million cubical, $3\text{mm} \times 3\text{mm} \times 3\text{mm}$ cells. Files of the field distributions in the main mesh were made for every plane 3-cm apart in the xy, yz and xz directions. For this report only a limited set of the most important distributions in planes identified by the black lines in Figures 3.1, 3.2 and 3.3 are illustrated in this. The black lines denoting the plotted fields in the x-y planes are labeled A through C, those denoting the plotted fields in the x-z planes are labeled D through F and those denoting the plotted fields in the y-z planes are labeled G through Q. The plane through G is aligned in contact and parallel to the front of the antenna radome, representing the closest distance that person could get to the radiating elements of the antenna. The plane through H is at a distance of 40-mm from the ground plane for which plots were made of the total electric and magnetic field as well as the x, y and z components to compare with the measurements discussed in Appendices A and B. The plane through M represents the closest distance, 200-mm, (within the nearest 2-mm) to the antenna at which power density can currently be used to determine compliance with the ANSI/IEEE (1991) and FCC MPLs of 1 mW/cm^2 . At closer distances measurements can suffer errors due to interaction of the measuring probe and the source. Also the fields tend to increase sharply with decreasing distance to the source in this region. Recently with the availability of better measurement probes, the IEEE SCC-28, promulgator of the ANSI/IEEE standard has voted to decrease this distance to 50-mm with the stipulation that if the standard is satisfied everywhere at that distance from the source, no further measurements are necessary for determining compliance with the standard. The plane where near fields were calculated for this distance (within the nearest 2-mm) is denoted by the letter, I. Currently, it is required by the FCC MPL to use average and peak specific absorption rates (SAR) in the exposed tissues to determine compliance in the region closer than 200-mm from most Personal Communications Service (PCS) devices emitting RF energy. The FCC SAR limits for the general population are 0.08 W/kg whole body average and 1.6 W/kg peak as averaged over a gram of tissue other than the limbs and 4 W/kg peak as averaged over 10 grams of tissue for the limbs.

5.2 *Electric Field Calculations and Measurements*

Figure 5.1 illustrates a color contour graph of the calculated near-zone electric field (E-field) along the plane denoted by G at the surface of the radome 31-mm from the surface of the ground plane. The color legend is scaled in dB with 0 dB corresponding to the maximum electric field strength of 49.1 V/m occurring near the lower right patch of the antenna at the location marked with a black plus sign. The electric field distribution closely matches those measured by SPEAG shown in Figure 2.11 on page 18 of Appendix A for a 30-mm distance from the ground plane. However the maximum amplitude for the latter is 58.6 V/m which is only 0.43 dB lower (page 16 of Appendix A) than the maximum 61.4 V/m allowed by the FCC MPL. The maximum amplitude of the calculated value is 0.85 dB lower than that allowed by the FCC MPL. The distribution also appears to be in good agreement with that measured by SARTest shown at the upper left of Figure 9 of Appendix B but the maximum magnitude of the latter was 68.5 V/m or 0.95 dB above the standard. One should keep in mind, however, that no standard is based on measurements in contact with an object such as the antenna radome. Compliance is based on measurements of 20 cm away from any object as now required by the ANSI/IEEE and FCC MPLs. The new ANSI/IEEE minimum measurement distance from any object that is a primary source of radiation (not a scatterer) will be 5 cm which is the distance used for measurements determining compliance with the U.S. Food and Drug Administration (FDA) microwave oven performance standard.

Figure 5.2 illustrates the graph of the calculated total E-field distribution and Figures 5.3, 5.4 and 5.5 illustrate the graphs of the respective x, y and z, E-field components at 40-mm from the antenna ground plane. The SPEAG measurements for these fields are illustrated in Figures 2.10 and 2.12 of Appendix A for 1 watt input power. For 79.62-mW input the SPEAG measured fields would be lower by a factor of 3.54. It also should be noticed that the SPEAG coordinate system x, y and z-axes correspond to the respective z, x and y axes in the XFDTD coordinate system. The measured distributions and magnitudes of the fields closely agree with the calculated values when the magnitude of the fields are normalized to the same input power and the field component directions are expressed in the same terms. Table 5.1 indicates that the total and principal vertical field values compare favorably within or close to the measurement accuracy's stated in Appendices A and B. The differences in the other field components are of little consequence since they are small compared with the total field and vary widely with small differences in antenna structure and orientation.

Table 5.1 Comparison from Different Laboratories of Maximum Calculated and Measured E-Field Strengths (V/m) in Plane Parallel to and 40-mm From Front of ATTWS RU Antenna Ground Plane with 79.62 mW Input Power at 1.92 GHz.

Laboratory	Total	Vertical field	Horizontal field	Normal field
BEMC (FDTD)	41.9	36.7	2.766	19.18
SPEAG (Measured)	40.0	36.3	12.2	27.7
SARTest (Measured)	49.0			

Figures 5.6 through 5.13 illustrate the respective color plots of the electric field (E-field) distribution in the yz planes for increasing values of x away from the antenna corresponding to planes I through O and Q as identified in Figures 3.1, 3.2 and 3.3. The legend for these plots and all remaining plots in this section is set to allow the color red to represent all field strengths at or greater than the value (61.4 V/m or 1 mW/cm² equivalent power density) specified by the FCC MPL.

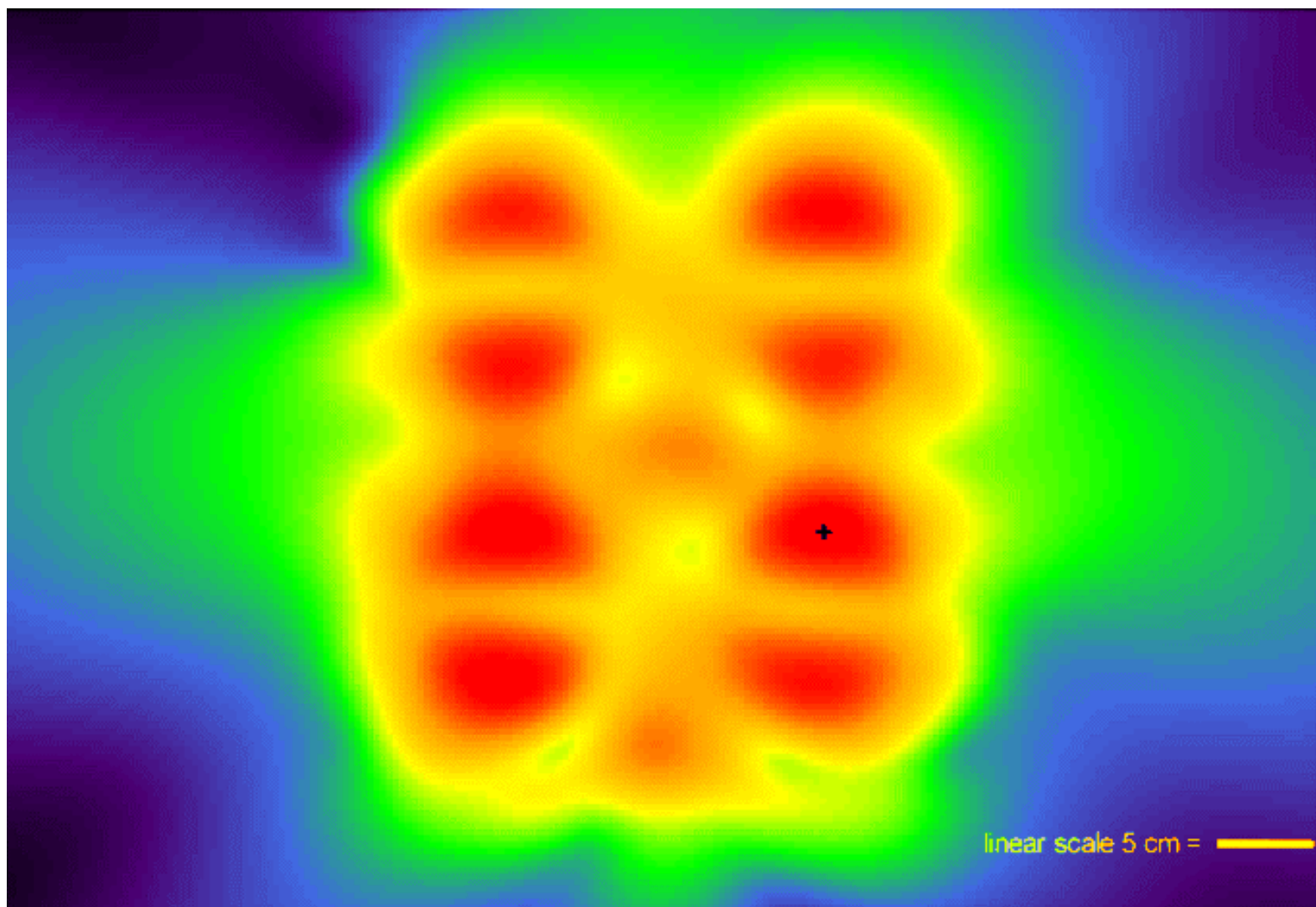
Figures 5.14 through 5.16 illustrate the respective color plots of the E-field distribution in the xy planes identified by A, B and C and Figures 5.17 through 5.19 illustrate the respective color plots of the E-field distribution in the xz plane identified by the lines D, E and F as identified in Figure 3.2.

It should be kept in mind that the outer edge of the red region away from the source in the xy and xz plane plots would correspond to less than the value of the MPL by one half the color increment (-3 dB) but at the inner region near the source, the fields can greatly exceed the FCC MPL since the color red represents an equivalent power density of 1 mW/cm² or greater. The other colors represent 6-decibel differences in field strengths or equivalent power density. Note that most of the color scales in the yz plots correspond to 3-decibel differences.

It can be seen from the xz and xy plane plots in Figures 5.14 through 5.19, that though the fields are high in the regions in and surrounding the antenna patch radiators, they decay very rapidly with distance from the source. The first red line in each graph represents the maximum outer extent of the radome of the antenna, which would be the closest proximity that a person could approach the radiating elements of the antenna. It is at least 2.0 cm from the nearest metal radiator of the antenna. The 2nd vertical red line marks the plane that is 5 cm from the surface of the antenna radome or 7.9 cm from the ground plane, beyond which measured or calculated power density is expected to be a valid metric for determining compliance with the new ANSI/IEEE MPL when it is published. We see from the E-field distribution in Figure 5.6 that the maximum calculated field at this distance is 28.2 V/m which is 6.76 dB below the FCC and the ANSI/IEEE MPLs of 61.4 V/m. The 3rd vertical red line marks the plane that is 20 cm from the surface of the antenna radome, beyond which measured or calculated power density is a valid metric for determining compliance with the current FCC MPL. The E-field distribution in Figure 5.10 indicates a maximum E-field of 29.89 V/m

at 20 cm from the antenna which is 6.25 dB below the FCC MPL. At distances closer than 20 cm from the antenna if the fields exceed the levels allowed by the MPL that would not necessarily mean that exposure to those fields would be out of compliance with the MPL. For such cases the calculated or measured SAR must be used to determine compliance. It can be seen from Figures 5.1 through 5.10 that the field strengths and equivalent power density within 20 cm from the antenna radome do not exceed levels allowed by the FCC exposure MPL. Never the less SAR calculations are needed to determine compliance with the FCC SAR MPL if exposures occur within the 20-cm distance from the antenna. It may be concluded that the field strengths at locations beyond the 20-cm line are 6 or more decibels below the FCC MPL.

The FDTD derived E-field data from the graphs discussed above are compared to the measurements made by SPEAG and SARTest (given in Appendices A and B) in Figure 5.20. The graph in Figure 5.20 shows the BEMC FDTD derived values as a solid blue line while the measurements are shown as symbols. Of the multiple SARTest measurement runs, both the highest and the lowest values are shown as open green squares while the SPEAG measurements are shown as solid red delta shaped symbols. The results of additional measurements made by BEMC in the ATTWS Antenna Laboratory anechoic chamber are shown as open orange squares. A Narda Model 8718 Survey meter with a model 8760 probe was used to do the ATTWS measurements. The probe may be too large to accurately measure the fields very close to the antenna, because of the finite size of the sensor as compared to highly divergent fields in this region. However, the probe should provide reasonably accurate results at distances of 5 to 20 cm or greater away from the antenna. A further comparison of the fields was made with theoretical far field calculations based on the 15.03-dBi gain of the antenna. The SPEAG (within 0.22 dB) and SARTest (within 1.8 dB at less than 40 mm from groundplane and 0.8 dB at greater than 40 mm from groundplane) measurements and the FDTD calculated results seem to agree very well within the measurement accuracy stated in Appendices A and B. The ATTWS measurements agree very well over the 20 and 50-cm distance in the transition region from the near field and the far field as well as in the far field. The calculated far field values based on the 15.03-dBi gain of the antenna agree with all of the other E-field data.



Scale 0 dB = 55.65 V/m

0	-6	-12	-18	-24
---	----	-----	-----	-----

Figure 5.1. FDTD derived E-field at surface of radome of AT&T RU antenna in y-z plane (Scan G, 31-mm from ground plane of antenna, maximum E-field denoted by black plus sign).